Antiswing Control and Trajectory Planning for Offshore Cranes

Ronny Landsverk
Faculty of Engineering and Science
University of Agder
Grimstad, Norway
ronny.landsverk@uia.no

Jing Zhou
Faculty of Engineering and Science
University of Agder
Grimstad, Norway
jing.zhou@uia.no

Daniel Hagen
Faculty of Engineering and Science
University of Agder
Grimstad, Norway
daniel.hagen@uia.no

***Abstract*—Safe handling of heavy payloads in an offshore environment requires careful crane maneuvering to avoid collision with obstacles and other equipment. The residual swing from a hanging payload can ultimately lead to danger and high cost failures if not properly dealt with. This paper investigates an open-loop control method for eliminating the payload swing for hanging loads on offshore knuckle-boom cranes. A trajectory tracking method is designed for payload swing suppression for open-loop control and based on the iterative learning algorithm. It is shown that the proposed anti-swing control method guarantees asymptotic convergence of the swing, the angular velocity, and the angular acceleration of the payload using Lyapunov techniques. The simulation results show the superior performance of the proposed anti-swing control method.**

***Index Terms*—antiswing control, crane, trajectory planning, screw kinematics, Lyapunov stability**

I. Introduction

Cranes are important for equipment handling and transportation in offshore industries such as drilling and assembly or operation of windmill farms. In harsh environments such as the North Sea, working safety is always of high priority. In a worst case scenario, a heavy lifting operation can impact vessel stability and dangerous situations and high-cost failures may follow.

Over the past decade, there has been significant research on the modeling and control of cranes. In [1], a Lagrangian-based dynamic model for a ship-mounted boom crane was introduced. Subsequent works built upon this by emphasizing offshore crane control in [2] and [3]. In [4], a moored crane-vessel with suspended load was analyzed both analytically and experimentally to study nonlinear dynamic phenomena affected by the mooring stiffness in particular. In [5] and [6], a fully coupled spatial knuckle-boom crane on a marine craft was modelled using Kane's method, using a minimal set of coordinates and generalized speeds. In above works, partial velocities needed for Kane's equations were defined as screws which enable screw transformations as a means to project kinetics to the inertial frame. In [7], a classical multi-body dynamics formulation was employed to derive a complete model of vessel, crane and payload, with a full set of Cartesian coordinates and Euler angles for each body, and including closed-loop kinetics that arise from linear actuators such as hydraulic cylinders.

For trajectory planning, approaches such as the cycloidal-based motion profiles for manipulators have been proposed for eliminating residual swing of a hanging payload [8], [9]. Effective swing elimination and precision in positioning for overhead cranes using Lyapunov-based analysis is illustrated in [10] and [11]. Furthermore, a blend of input shaping with closed-loop control has been implemented for swing elimination in an offshore boom crane [12]. Other methods include energy-based nonlinear controls [13]–[15] and adaptive controls [16]–[18].

In this paper, a trajectory tracking method is implemented for payload swing suppression for open-loop control of offshore cranes. The control objective is to transport the load to the desired location quickly and precisely, while suppressing the payload swing simultaneously. The method is based on an iterative learning algorithm developed for overhead cranes [10], by employing an antiswing mechanism to manipulate a smooth reference trajectory. The iterative learning converges rapidly, making it feasable for implementation on existing offshore crane applications. The method is useful in industrial applications, since it will increase transportation efficiency and secure safety in a high risk working environment. Furthermore, as this is an open loop method, there is no requirement for sensor feedback from the payload. It is shown that the proposed anti-swing control method guarantees asymptotic convergence of the swing, the angular velocity, and the angular acceleration of the payload using Lyapunov techniques. The simulation results show the superior performance of the proposed anti-swing control method. The main contribution is the application of techniques from paper [10] to a spatial knuckle boom crane rather than the traditional planar overhead crane.

The rest of this paper is structured as follows. Section II presents dynamics model of crane systems. Section III proposes the antiswing control method. Section IV

The research presented in this paper has received funding from the Norwegian Research Council, SFI Offshore Mechatronics, project number 237896.

evaluates the performance of the proposed method and presents the simulation results. Section V concludes the paper.

II. Modeling of Crane System

In this paper, an open serial link manipulator with three revolute joints is considered. Such a manipulator will capture the essential dynamics of a typical offshore knuckle-boom crane if we replace two linear actuators (see hydraulic cylinders in [7]) by rotary actuators placed at the joints.

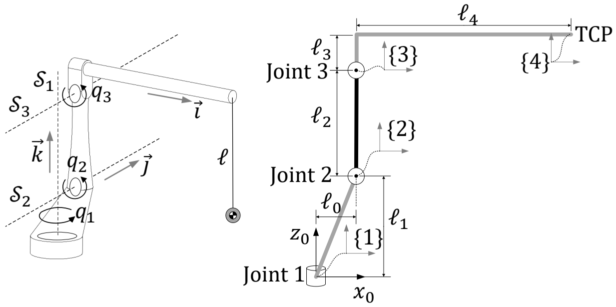

Fig. 1: Serial manipulator crane

Fig. 1 shows the considered system, parameterized by lengths ℓ_i, $i = \{0,1,2,3,4\}$ and joint angles q_j, $j = \{1,2,3\}$. The forward kinematics from the base frame $\{0\}$ to the tool frame $\{4\}$ can be written in terms of the screws $\mathcal{S}_i$ and joint variables $\mathbf{q}$, as shown in Fig. 1,

$$\mathcal{S}_1 = \begin{bmatrix} \mathbf{w}_1 \\ \mathbf{v}_1 \end{bmatrix},\ \mathcal{S}_2 = \begin{bmatrix} \mathbf{w}_2 \\ \mathbf{v}_2 \end{bmatrix},\ \mathcal{S}_3 = \begin{bmatrix} \mathbf{w}_3 \\ \mathbf{v}_3 \end{bmatrix},\ \mathbf{q} = \begin{bmatrix} q_1 \\ q_2 \\ q_3 \end{bmatrix}, \tag{1}$$

where $\mathbf{w}_i \in \mathbb{R}^3$ is a unit vector pointing along the screw axis $\mathcal{S}_i \in \mathbb{R}^6$ and $\mathbf{v}_i \in \mathbb{R}^3$ is the negative kinematic moment of the screw axis at an arbitrary point $\mathbf{p}_i \in \mathbb{R}^3$ on the screw axis.

$$\mathbf{v}_i = -\mathbf{w}_i \times \mathbf{p}_i, \qquad i = \{1,2,3\} \tag{2}$$

Then we define the matrix $\mathbf{T} = \mathbf{T}(\mathbf{q}) \in SE(3)$ which acts as the transformation from $\{0\}$ to $\{4\}$ in the base frame

$$\mathbf{T}(\mathbf{q}) = \mathbf{exp}(\tilde{\mathcal{S}}_1 q_1)\mathbf{exp}(\tilde{\mathcal{S}}_2 q_2)\mathbf{exp}(\tilde{\mathcal{S}}_3 q_3)\mathbf{T}(\mathbf{0}), \tag{3}$$

where the tilde notation denotes transforming a screw to an element in $se(3)$ - representing the Lie algebra for the special Euclidian group $SE(3)$, and transforms a vector to an element in $so(3)$ - representing the Lie algebra for the special orthogonal group $SO(3)$, both according to

$$\tilde{\mathcal{S}} = \begin{bmatrix} \tilde{\mathbf{w}} & \mathbf{v} \\ \mathbf{0} & 0 \end{bmatrix} \in se(3) \tag{4}$$

$$\tilde{\mathbf{w}} = \begin{bmatrix} 0 & -w_3 & w_2 \\ w_3 & 0 & -w_1 \\ -w_2 & w_1 & 0 \end{bmatrix} \in so(3) \tag{5}$$

and the operator $\mathbf{exp}$ denotes the matrix exponential

$$\mathbf{exp}(\mathbf{A}) = e^{\mathbf{A}} = \mathbf{I} + \frac{1}{2!}\mathbf{A}^2 + \frac{1}{3!}\mathbf{A}^3 + \cdots + \frac{1}{k!}\mathbf{A}^k + \cdots \tag{6}$$

Finally, $\mathbf{T}(\mathbf{0})$ denotes the element in $SE(3)$ that describes the pose of frame $\{4\}$ relative to $\{0\}$ when all joint variables are zero.

To implement the antiswing signal, we need to first specify a trajectory for the tool centre point (TCP) of the crane in base frame coordinates, and transform this trajectory from the cartesian tool space to the joint space. Note that the base frame $\{0\}$ is an inertial frame, and the TCP is the origin of frame $\{4\}$. The inverse kinematics (Fig. 2) can easily be determined by employing a small trick to account for the offset ℓ_3 between joint 3 and frame $\{4\}$.

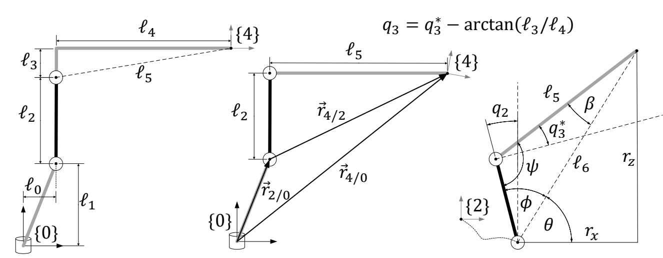

Fig. 2: Inverse kinematics

By defining joint variable $q_3 = q_3^* - \arctan(\ell_3/\ell_4)$ and link length $\ell_5 = \sqrt{\ell_3^2 + \ell_4^2}$ then given any TCP position $\vec{r}_{4/0} = (p_x, p_y, p_z)$, where the notation $\vec{r}_{j/i}$ specifies a geometric vector from frame $\{i\}$ to $\{j\}$, we can write

$$q_1 = \arctan(p_y/p_x) \tag{7}$$

Once we have q_1 we can rotate the TCP vector $\vec{r}_{4/0}$ by angle $(-q_1)$ about $\vec{k}$ such that the robot aligns with the base x axis. This effectively will turn the vector $\vec{r}_{4/0}$ into a planar vector in the (x,z)-plane, and using the center picture of Fig. 2 we write

$$\vec{r}_{4/2} = \vec{r}_{4/0} - \vec{r}_{2/0} = (r_x, r_z) \tag{8}$$

Finally, using the rightmost picture of Fig. 2, we get the relations

$$\frac{\pi}{2} + q_2 = \theta + \phi, \qquad \frac{\pi}{2} + q_3^* = \psi \tag{9}$$

where

$$\phi = \arccos\left(\frac{\ell_2^2 + \ell_6^2 - \ell_5^2}{2\ell_2\ell_6}\right) \tag{10}$$

and

$$\psi = \arccos\left(\frac{\ell_2^2 + \ell_5^2 - \ell_6^2}{2\ell_2\ell_5}\right) \tag{11}$$

where $\ell_6 = \sqrt{r_x^2 + r_z^2}$ and $\theta = \arctan(r_z/r_x)$. Note that we also need to account for poses that have two equally valid solutions in joint space, i.e. elbow up/down.

For the relation between TCP velocity $\mathbf{v} = \dot{\mathbf{r}}$, where $\mathbf{r}$ is the algebraic form of the vector $\vec{r}_{4/0}$, and joint velocities $\dot{\mathbf{q}}$ we need to derive the Jacobian $\mathbf{J} = \mathbf{J}(\mathbf{q})$

$$\mathbf{v} = \mathbf{J}(\mathbf{q})\dot{\mathbf{q}} \tag{12}$$

The Jacobian can be written

$$\mathbf{J} = \begin{bmatrix} \mathbf{J}_1 & \mathbf{J}_2 & \mathbf{J}_3 \end{bmatrix} \in \mathbb{R}^{3\times 3} \tag{13}$$

where

$$\mathbf{J}_i = \mathbf{w}_i \times (\mathbf{r} - \mathbf{r}_{i/0}), \qquad i = \{1, 2, 3\} \tag{14}$$

where $\mathbf{r}_{j/i}$ denotes the algebraic vector from frame $\{i\}$ to $\{j\}$ in frame $\{0\}$ coordinates. Furthermore $\mathbf{r} = \mathbf{r}_{4/0}$, and $\mathbf{w}_i$ is a unit vector in the positive direction along the axis of joint i, also in frame $\{0\}$ coordinates. Differentiating Eq. (12) w.r.t. time yields

$$\dot{\mathbf{v}} = \frac{\partial \mathbf{J}}{\partial \mathbf{q}}\dot{\mathbf{q}}^2 + \mathbf{J}(\mathbf{q})\ddot{\mathbf{q}} = \mathbf{J}_{\mathbf{q}}(\mathbf{q})\dot{\mathbf{q}}^2 + \mathbf{J}(\mathbf{q})\ddot{\mathbf{q}} \tag{15}$$

Note that the Jacobian and it's partial derivative $\mathbf{J}_{\mathbf{q}}$ are square and nonsingular in our interval of interest, so the inverse kinematics for velocities and accelerations may follow directly from equations (12) and (15) while keeping the workspace within this interval.

The control objective is to accurately position the TCP from a point A to a point B in a specified time T_f - starting and ending the trajectory with zero velocity and acceleration - while simultaneously suppressing the residual swing from the hanging load.

III. Antiswing Control

A. Trajectory Planning

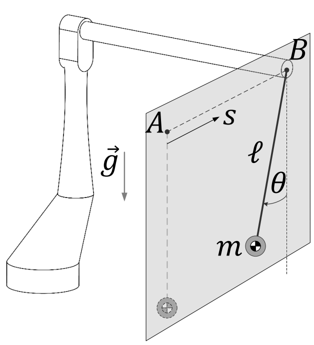

Fig. 3: Considered system - crane and payload

Fig. 3 depicts a situation where the hanging load is moved from point A to point B along a horizontal straight line. The plane in the figure highlights that the pendulum dynamics is essentially planar and assuming no friction, the governing equation for the payload can be written

$$m\ell\ddot{s}\cos(\theta) + m\ell^2\ddot{\theta} = -mg\ell\sin(\theta) \tag{16}$$

where m is the payload mass, ℓ is the pendulum length, g is the gravitational constant and θ and s are state variables. Note that s is the distance along the line $s_B - s_A = \|\mathbf{r}_B - \mathbf{r}_A\|$ where $\mathbf{r}_A$ is the component vector for $\vec{r}_{4/0}$ when the TCP is located at point A and similarly for $\mathbf{r}_B$. Dividing Eq. (16) by $m\ell$ yields the equation

$$\ell\ddot{\theta} + \ddot{s}\cos(\theta) + g\sin(\theta) = 0 \tag{17}$$

Eq. (17) forms the basis for designing a swing elimination signal - hereby denoted as the antiswing signal.

The primary control goal is for the TCP position s to reach a specified position p without overshoot in time T_f. The state s and it's derivatives up to third order must be uniformly bounded with $\dot{s} \geq 0$, $|\ddot{s}| < g$ and $\dot{s}(T_f) = \ddot{s}(T_f) = 0$.

B. Iterative Learning Algorithm

First, based on [10] we specify a linear filter

$$\sigma = \dot{\theta} + \alpha\theta \tag{18}$$

where $\alpha \in \mathbb{R}$, and define the antiswing signal as

$$\ddot{s}_a = \frac{-g\sin(\theta) + \alpha\ell\dot{\theta} + \beta\sigma}{\cos(\theta)} \tag{19}$$

where $\beta \in \mathbb{R}$. The TCP reference trajectory is combined with the anti-swing signal as

$$\ddot{s} = \ddot{s}_{\text{ref}} + \gamma\ddot{s}_a \tag{20}$$

where $\gamma \in \mathbb{R}$ is a gain factor and $\ddot{s}_{\text{ref}}$ is a smooth trajectory acceleration reference. By taking the derivative of the filter (Eq. 18) and using the dynamics in Eqs. (17), (19), the filter can be written $\sigma = C\mathrm{e}^{-\beta t/\ell}$, which shows that $\theta, \dot{\theta}$ decays exponentially fast. Based on the analysis [10], using Lyapunov function

$$V(t) = \frac{1}{2}\ell\dot{\theta}^2 - g(1 - \cos(\theta)) \tag{21}$$

and Barbalat's lemma, the antiswing signal (19) and the reference trajectory (20) can be shown to suppress the payload swing successfully and efficiently. The results are shown in the following theorem.

Theorem 1. *The combined anti-swing mechanism (19) and the reference trajectory (20) guarantees asymptotic convergence of the swing, the angular velocity, and the angular acceleration of the payload, such that*

$$\lim_{t\to\infty} \left(\theta(t), \dot{\theta}(t), \ddot{\theta}(t)\right) = (0, 0, 0) \tag{22}$$

Proof: The results are obtained using Luapunov techniques, Barbalat's lemma and extended Barbalat's lemma. More detailed analysis is given in [10].

The system shown in Fig. 4 is depicting the main building blocks that make up a single iteration in the iterative learning procedure. The block *Antiswing* consists of the antiswing signal, dependent on parameters α, β and state variables θ and $\dot{\theta}$. The block *Trajectory* is responsible for generating a smooth trajectory for the TCP, i.e. for $s_r, \dot{s}_r$, and $\ddot{s}_r$ with boundary conditions $\dot{s}_r(0) = \ddot{s}_r(0) =$

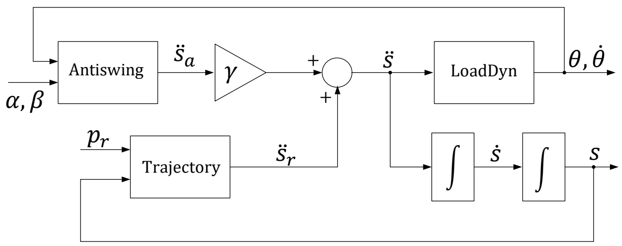

Fig. 4: Sub-system for iterative learning

$\dot{s}_r(T_f) = \ddot{s}_r(T_f) = 0$. The block is dependent on the parameters p_r, T_f, and state variable s. Note that T_f is a constant, and p_r is an optimization variable for the algorithm. The block *LoadDyn* consists of the pendulum dynamics (17), and is straightforward.

Fig. 5 shows the overall learning strategy, utilizing the sub-system shown in Fig. 4 for each iteration k. The error

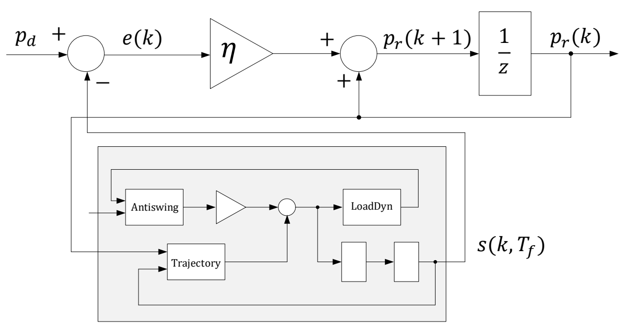

Fig. 5: Overall learning strategy

$e(k)$ is the difference between the desired final position $s(T_f) \approx p_d$ and the final position of the previous step, denoted by $s(k, T_f)$.

$$e(k) = p_d - s(k, T_f) \tag{23}$$

The variable $p_r(k)$ is used as a total displacement-input for the trajectory generator during iteration k, and gets updated for the next iteration by

$$p_r(k+1) = \eta e(k) + p_r(k) \tag{24}$$

where η governs the rate of convergence. It's easy to see that as $e(k) \to 0$, the iterative algorithm stabilizes for a suitable $p_r(k+1) \approx p_r(k)$.

IV. Simulation Results

A. Implementing Anti-swing in Cartesian 3-Space

As a specific case for our model, we choose an initial pose of $q_1 = -50°$, $q_2 = 60°$ and $q_3 = -60°$. The pose is shown in Fig. 6, with the TCP positioned at point A .

Suppose we want to move the TCP by a distance of $(s_B - s_A) = \delta s = \sqrt{\delta x^2 + \delta y^2 + \delta z^2}$ moving twice the distance in the y direction as in the x direction, while keeping the z-component constant. Then $\delta s = \sqrt{\delta x^2 + 4\delta x^2}$.

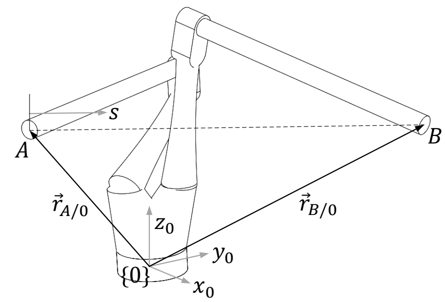

Fig. 6: Initial and final pose

Choosing $\delta s = 3$ m we get $\delta x = 3/\sqrt{5}$, $\delta y = 6/\sqrt{5}$ and $\delta z = 0$. For lengths $\ell_0 = 0.35$ m, $\ell_1 = 0.83$ m, $\ell_2 = 1.16$ m, $\ell_3 = 0.25$ m, and $\ell_4 = 2.27$ m, the initial and final poses are as shown in Fig. 6.

The final pose of the robot at point B is calculated using inverse kinematics and the TCP position at point A is calculated using forward kinematics

$$\mathbf{r}_A = \begin{bmatrix} -1.038 \\ -1.237 \\ 1.66 \end{bmatrix}, \qquad \mathbf{r}_B = \mathbf{r}_A + \begin{bmatrix} \delta x \\ \delta y \\ 0 \end{bmatrix}$$

The joint position values that correspond to pose B are $q_1 = 31.3°$, $q_2 = -8.62°$, and $q_3 = -5.64°$.

B. Results

To test the effectiveness of the anti-swing control, we compare the swing attenuation for a fifth-order polynomial trajectory

$$\begin{aligned} s(t) &= a_0 + a_1 t + a_2 t^2 + a_3 t^3 + a_4 t^4 + a_5 t^5 \\ \dot{s}(t) &= a_1 + 2a_2 t + 3a_3 t^2 + 4a_4 t^3 + 5a_5 t^4 \\ \ddot{s}(t) &= 2a_2 + 6a_3 t + 12a_4 t^2 + 20a_5 t^3 \end{aligned} \tag{25}$$

with $s(0) = \dot{s}(0) = \dot{s}(3) = \ddot{s}(0) = \ddot{s}(3) = 0$ and $s(3) = p_d = 3$, against a trajectory where the antiswing signal is included.

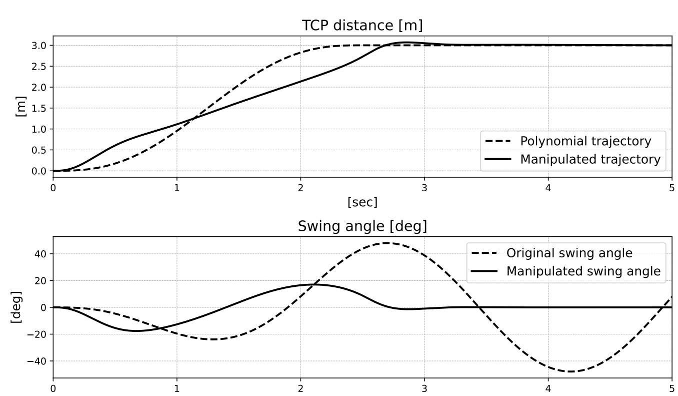

Fig. 7: TCP displacement and payload swing angle

The TCP displacement along s is shown in the upper plot and the payload swing angle is shown in the lower plot of Fig. 7. The solid and dashed lines are simulation results with and without the antiswing signal. We see that the residual swing is effectively eliminated during the positioning of the payload, which is at a final position at time $t \approx 3.0$ sec. Note that the so-called *smooth* polynomial trajectory will yield a $\pm 45°$ swinging motion lasting forever in a friction-less environment.

Fig. 8 shows the error $e(k) = p_d(k) - s(k, T_f)$ for iterations $k = 1, 2, ..., 11$ with a learning rate $\eta = 3.5$. Furthermore, the parameters α, β and γ in equations (18), (19) and (20) are chosen rather randomly as $\alpha = \beta = 20$ and $\gamma = 0.3$. Further recommendations for choosing suitable numbers can be found in [10].

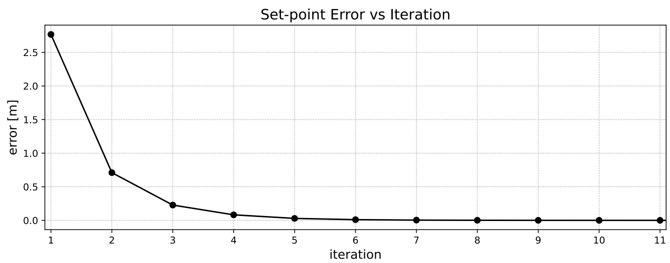

Fig. 8: Setpoint error vs iterations

The effectiveness and validity of the implementation of the antiswing signal to the crane system, and the system modeling shown in this paper, are verified by feeding trajectory references derived from the modeling as joint references for a MATLAB Simulink Simscape MBS model of the robot. Based on the cartesian trajectory that realizes the TCP displacement in Fig. 7, we find trajectories in the joint space as shown in Fig. 9.

The joint positions $\mathbf{q}(t) \in \mathbb{R}^3$ are readily found using the inverse kinematics from Eqs. (7), (9), (10) and (11), based on the desired starting TCP position $\mathbf{r}(0) = \mathbf{r}_A$ and the chosen direction of path variable s. The joint velocities and accelerations are calculated from

$$\dot{\mathbf{q}}(t) = \mathbf{J}^{-1}(\mathbf{q})\mathbf{v}(t) \tag{26}$$

and

$$\ddot{\mathbf{q}}(t) = \mathbf{J}^{-1}(\mathbf{q}) \left(\dot{\mathbf{v}}(t) - \mathbf{J_q}(\mathbf{q})\dot{\mathbf{q}}^2(t) \right) \tag{27}$$

where $\mathbf{J} \in \mathbb{R}^{3\times3}$ and $\mathbf{J_q} \in \mathbb{R}^{3\times3}$ are the geometric Jacobian and it's partial derivative, and $\mathbf{v} \in \mathbb{R}^3$, $\dot{\mathbf{v}} \in \mathbb{R}^3$ are the velocity and acceleration of the TCP in cartesian 3-space. The joint references for position, velocity and acceleration are tested for validity in the Simscape-MBS model shown in Fig. 11.

The payload block consisting of the pendulum dynamics is attached to the TCP of the crane model block via a spherical joint. Both the position, velocity and acceleration of the TCP of the crane, and the payload swing angle are measured and verified to correspond with the calculated trajectories as shown in Fig. 10, for which the upper plot shows the TCP position in cartesian coordinates and the lower plot shows the swing angles - comparing the desired outcome denoted as *Model* against the simulated result denoted as *Simscape*.

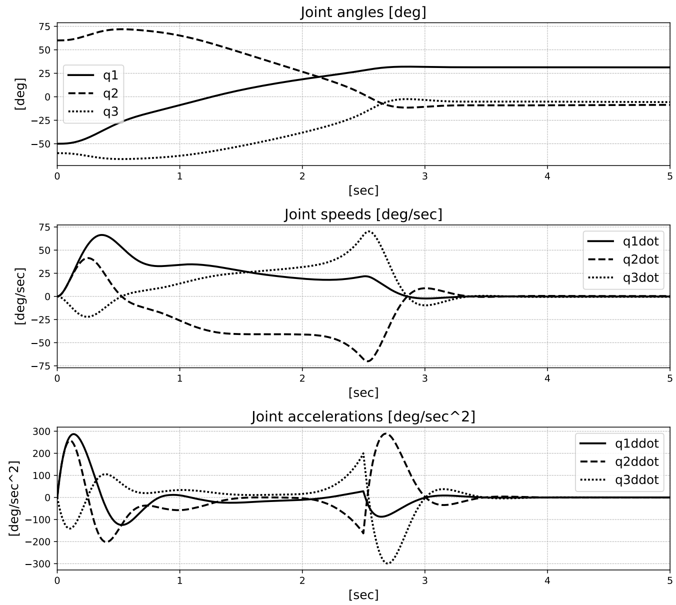

Fig. 9: Joint trajectories

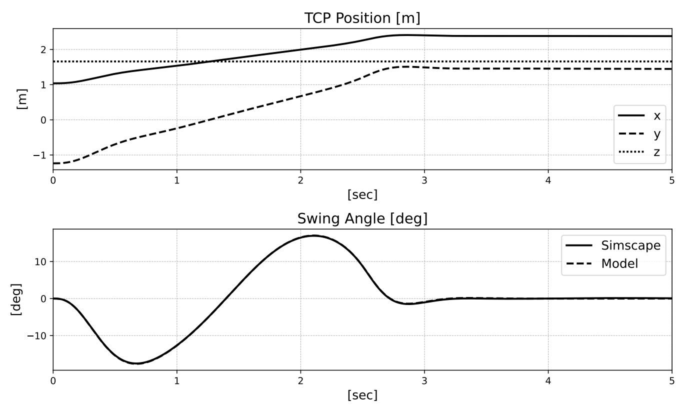

Fig. 10: Simscape simulation results

A recorded animation of the Simscape model for comparing the responses with and without the antiswing signal can be viewed at [19].

V. Conclusion

This paper presents the implementation of an iterative open-loop control algorithm developed for overhead cranes on a serial manipulator that represents a knuckle-boom crane. The controller effectively removes the residual swinging motion imposed from moving a hanging payload. The algorithm will be tested experimentally on a Comau manipulator mounted on a Stewart-Platform in the near

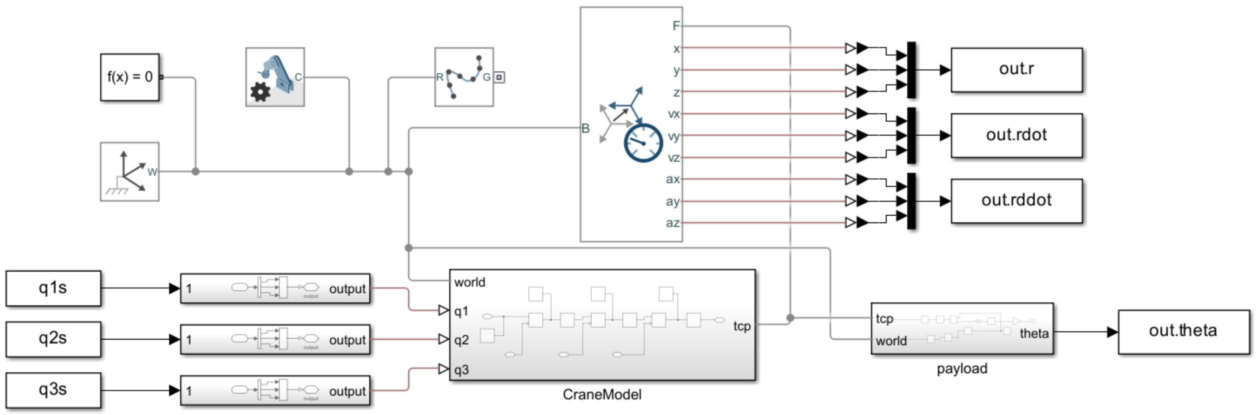

Fig. 11: Main blocks in Simscape MBS

future and further investigated for integration in a closed-loop control system for realistic antiswing compensation for an offshore vessel-mounted knuckle-boom crane under disturbance from wave motion.

Acknowledgment

The research presented in this paper has received funding from the Norwegian Research Council, SFI Offshore Mechatronics, project number 237896.

References

[1] Y. Fang, P. Wang, N. Sun, and Y. Zhang, "Dynamic Analysis and Nonlinear Control of an Offshore Boom Crane," *IEEE Transactions on Industrial Electronics*, pp. 414–426, 2014.

[2] Y. Qian and Y. Fang, "Dynamic Analysis of an Offshore Ship-mounted Crane Subject to Sea Wave Disturbances," *IEEE World Congress on Intelligent Control and Automation*, pp. 1251–1256, 2016.

[3] B. Lu, Y. Fang, N. Sun, and X. Wang, "Antiswing Control of Offshore Boom Cranes with Ship Roll Distrurbances," *IEEE Transactions on Control Systems Technology*, pp. 740–747, 2018.

[4] K. Ellerman, E. Kreuzer, and M. Markiewitcz, "Nonlinear Dynamics of Floating Cranes," *Nonlinear Dynamics*, vol. 27, pp. 377–387, 2002.

[5] G. Tysse and O. Egeland, "Dynamic Interaction of a Heavy Crane and a Ship in Wave Motion," *Modeling, Identification and Control*, vol. 39, pp. 45–60, 2018.

[6] A. Cibicik, G. Tysse, and O. Egeland, "Determination of Reaction Forces of a Deck Crane in Wave Motion Using Screw Theory," *Journal of Offshore Mechanics and Arctic Engineering*, vol. 141, pp. 1–12, 2019.

[7] R. Landsverk, J. Zhou, G. Hovland, and H. Zhang, "Modeling of Offshore Crane and Marine Craft in Wave Motion," *15th IEEE Conference on Industrial Electronics and Applications (ICIEA)*, pp. 1463–1470, 2020.

[8] G. Alici, S. Kapucu, and S. Bayseç, "Swing-free transportation of suspended objects with robot manipulators," *Robotica*, vol. 17, no. 5, p. 513–521, 1999.

[9] A. Gürsel, S. Kapucu, and S. Bayseç, "On preshaped reference inputs to reduce swing of suspended objects transported with robot manipulators," *Mechatronics*, vol. 10, no. 6, pp. 609–626, 2000.

[10] Y. Z. N. Sun, Y. Fang and B. Ma, "A Novel Kinematic Coupling-Based Trajectory Planning Method for Overhead Cranes," *IEEE Transactions on Mechatronics*, 2012.

[11] N. Sun and Y. Fang, "An efficient online trajectory generating method for underactuated crane systems," *Int. J. Robust Nonlinear Control*, vol. 24, pp. 1653–1663, 2014.

[12] M. Agostini, G. Parker, K. Groom, H. Schaub, and R. Robinett, "Command Shaping and Closed-Loop Control Interactions for a Ship Crane," *Proceedings of the 2002 American Control Conf.*, vol. 5, pp. 2298–2304, 2002.

[13] N. Sun, Y. Wu, Y. Fang, and H. Chen, "Nonlinear Antiswing Control for Crane Systems with Double-Pendulum Swing Effects and Uncertain Parameters: Design and Experiments," *IEEE Transactions on Automation Science and Engineering*, vol. 15, no. 3, pp. 1413–1412, 2018.

[14] N. Sun, Y. Wu, and L. Xiao, "Nonlinear Stable Transportation Control for Double-Pendulum Shipboard Cranes with Ship-Motion-Induced Disturbances," *IEEE Transactions on Industrial Electronics*, vol. 66, no. 12, pp. 9467–9479, 2019.

[15] H. Chen and N. Sun, "An Output Feedback Approach for Regulation of 5-DOF Offshore Cranes with Ship Yaw and Roll Perturbations," *IEEE Transactions on Industrial Electronics*, vol. 69, no. 2, pp. 1705–1716, 2022.

[16] J. Gao, L. Wang, R. Gao, and J. Huang, "Adaptive control of uncertain underactuated cranes with a non-recursive control scheme," *Journal of the Franklin Institute*, vol. 356, no. 18, pp. 11 305–11 317, 2019.

[17] N. Sun, T. Yang, H. Chen, Y. Fang, and Y. Qian, "Adaptive anti-awing and positioning control for 4-dof rotary cranes subject to uncertain/unknown parameters with hardware experiments," *IEEE Transactions on Systems, Man, and Cybernetics: Systems*, vol. 49, pp. 1309–1321, 2019.

[18] J. Huang, W. Wang, and J. Zhou, "Adaptive Control Design for Underactuated Cranes With Guaranteed Transient Performance: Theoretical Design and Experimental Verification," *IEEE Transactions on Industrial Electronics*, vol. 69, no. 3, pp. 2822–2832, 2022.

[19] R. Landsverk, "Clipchamp Video of Simscape Simulation," https://clipchamp.com/watch/6ZHXOAI3Eio.